Nonlinear Dyn (2021) 103:2409–2420
https://doi.org/10.1007/s11071-021-06254-0

ORIGINAL PAPER

Non-prehensile manipulation of a devil-stick: planar symmetric juggling using impulsive forces

Nilay Kant · Ranjan Mukherjee

Received: 27 July 2020 / Accepted: 22 January 2021 / Published online: 15 February 2021

Abstract Juggling a devil-stick can be described as a problem of non-prehensile manipulation. Assuming that the devil-stick remains confined to the vertical plane, the problem of juggling the stick between two symmetric configurations is considered. Impulsive forces are applied to the stick intermittently and the impulse of the force and its point of application are modeled as control inputs to the system. The dynamics of the devil-stick due to the impulsive forces and gravity is described by half-return maps between two Poincaré sections; the symmetric configurations are fixed points of these sections. A coordinate transformation is used to convert the juggling problem to that of stabilization of one of the fixed points. Inclusion of the coordinate transformation in the dynamic model results in a nonlinear discrete-time system. A dead-beat design for one of the inputs simplifies the control problem and results in a linear time-invariant discrete-time system. Standard control techniques are used to show that symmetric juggling can be achieved from arbitrary initial conditions.

Keywords Devil-stick · Dynamics · Impulsive force · Juggling · Non-prehensile manipulation · Poincaré map

N. Kant · R. Mukherjee (✉)
Mechanical Engineering Department, Michigan State University, East Lansing, MI 48824, USA
e-mail: mukherji@egr.msu.edu

N. Kant
e-mail: kantnila@msu.edu

1 Introduction

A devil-stick is typically juggled using two hand sticks and several tricks can be performed depending on the proficiency of the juggler. Some of the common tricks are: *standard-idle*, *flip-idle*, *airplane-spin* or *propeller*, *top-only idle*, and *helicopter* [1]. The *top-only idle* is one of the simplest tricks and is the focus of this investigation; a video tutorial for learning this trick can be found in [2]. In top-only idle, intermittent forces are applied to the devil-stick. Since the devil-stick is never grasped, the juggling problem can be viewed as a non-prehensile manipulation problem [3–7]. If robots are to perform this trick, the motion of the end-effectors will have to be coordinated and controlled to apply the correct magnitude of forces to the devil-stick at appropriate locations. We do not focus on the end-effector motion planning and control problems; instead, we investigate the magnitude and location of the forces needed to perform the *top-only idle* trick.

It should be mentioned that the complete problem, where the manipulator and the object being juggled are both controlled, has been studied by several researchers—see [8–11], for example. In one of the earliest works, Brogliato and Zavala Rio [11] investigated the problem of ball juggling using a controlled one-DOF table that imparts intermittent impulsive forces. This work was later extended to develop a feedback control method for complementary-slackness hybrid

mechanical systems; ball juggling using a two-DOF manipulator was demonstrated through simulations [8].

Many control tasks, including the *top-only idle* trick, involve intermittent application of impulsive forces and several researchers [12–17] have studied the controllability and stability of such systems. Although impulsive control of the devil-stick has not been investigated, the control problem associated with juggling of balls and air-hockey pucks has seen several solutions [8,11,18–21]. In all of these solutions, the object being juggled has been modeled as a point mass and its orientation is excluded from the dynamic model. In contrast, for devil-stick tricks such as *top-only idle*, the stick is shuffled between two symmetric configurations about the vertical; therefore, the orientation of the stick must be included in the dynamic model.

In earlier works on the devil-stick [22,23], controllers have been designed for *airplane-spin* or *propeller*-type motion; a single hand-stick is used to rotate the devil-stick about a virtual horizontal axis using continuous-time inputs. The dynamics model and control design of *top-only idle* motion of the devil-stick has not appeared in the literature; to the best of our knowledge, it is presented here for the first time. It is assumed that impulsive forces are applied intermittently to the devil-stick and the control inputs are the impulse of the force and its point of application on the stick. The control inputs are designed to juggle the stick between two symmetric configurations about the vertical, starting from an arbitrary initial configuration.

This paper is organized as follows. The juggling problem is formally described in Sect. 2. The dynamics of the devil-stick is presented in Sect. 3; it is comprised of impulsive dynamics due to the control inputs and continuous dynamics due to torque-free motion under gravity. A coordinate transformation is used to simplify the control problem and the dynamics is described by a nonlinear discrete-time system. The control design is provided in Sect. 4. By choosing one of the control inputs to be dead-beat, the nonlinear system is simplified to a linear discrete-time system. For stable juggling, the linear system is controlled using linear quadratic regulator (LQR) and model predictive control (MPC) techniques. Simulation results are presented in Sect. 5 and concluding remarks are provided in Sect. 6.

2 Problem description

Consider the three degree-of-freedom devil-stick shown in Fig. 1, which can move freely in the xy vertical plane. The stick has length ℓ, mass m, and mass moment of inertia J about its center-of-mass G. The configuration of the stick is described by the three generalized coordinates: (θ, h_x, h_y), where θ is the orientation of the stick with respect to the positive x-axis, measured counterclockwise, and (h_x, h_y) are the Cartesian coordinates of G. The objective is to juggle the stick between two configurations that are symmetric with respect to the vertical axis. The coordinates of the stick in these two configurations are (θ^*, h_x^*, h_y^*) and $(\pi - \theta^*, -h_x^*, h_y^*)$, where $\theta^* \in (0, \pi/2)$—see Fig. 2. It is assumed that juggling is achieved by applying impulsive forces perpendicular to the stick; they are applied only when the orientation of the stick is $\theta = \theta^*$ or $\theta = \pi - \theta^*$. Therefore, the time of application of the impulsive force is not a part of the control design. The control inputs are the pair (I, r), where I, $I \geq 0$, is the impulse of the impulsive force and r is the distance of the point of application of the force from G. The value of r is considered to be positive if the angular impulse of the impulsive force about G is in the positive z direction when $\theta = \theta^*$, and is in the negative z direction when $\theta = \pi - \theta^*$. The control inputs that juggle the stick

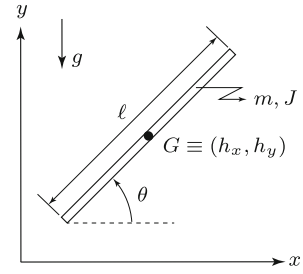

Fig. 1 A three degree-of-freedom devil stick

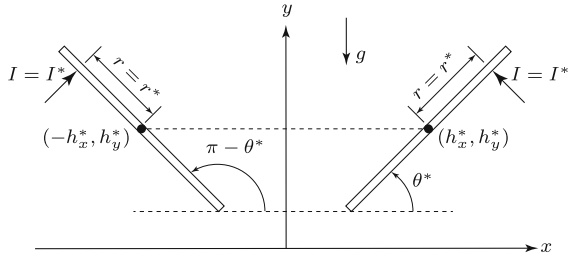

Fig. 2 Symmetric configurations of the devil-stick in Fig. 1

between the symmetric configurations are denoted by the pair (I^*, r^*).

3 Dynamics of the devil-stick

3.1 Impulsive dynamics

The dynamics of the three-DOF devil-stick is described by the six-dimensional state vector X, where

$$X = \begin{bmatrix} \theta & \omega & h_x & v_x & h_y & v_y \end{bmatrix}^T, \quad \omega \triangleq \dot{\theta}, \quad v_x \triangleq \dot{h}_x, \quad v_y \triangleq \dot{h}_y$$

Let $t_k, k = 1, 2, 3, \cdots$, denote the instants of time when the impulsive inputs are applied. Furthermore, without loss of generality, let $k = (2n-1)$, $n = 1, 2, \cdots$ denote the instants of time when the impulsive inputs are applied at $\theta = \theta^*$, and $k = 2n, n = 1, 2, \cdots$ denote the instants of time when the impulsive inputs are applied at $\theta = \pi - \theta^*$. If t_k^- and t_k^+ denote the instants of time immediately before and after application of the impulsive inputs, the linear and angular impulse-momentum relationships can be used to describe the impulsive dynamics[1] as follows, for $k = 1, 3, 5, \cdots$

$$X(t_k^+) = X(t_k^-) + \begin{bmatrix} 0 \\ (I_k\, r_k/J) \\ 0 \\ -(I_k/m)\sin\theta^* \\ 0 \\ (I_k/m)\cos\theta^* \end{bmatrix} \tag{1}$$

and for $k = 2, 4, 6, \cdots$

$$X(t_k^+) = X(t_k^-) + \begin{bmatrix} 0 \\ -(I_k\, r_k/J) \\ 0 \\ (I_k/m)\sin\theta^* \\ 0 \\ (I_k/m)\cos\theta^* \end{bmatrix} \tag{2}$$

where (I_k, r_k) denote the control inputs at time t_k. Between two consecutive impulsive inputs, the devil-stick undergoes torque-free motion under gravity; this is discussed next.

[1] Impulsive inputs cause discontinuous jumps in the velocity coordinates but no change in the position coordinates [24]. The dynamics of underactuated systems subjected to impulsive inputs is discussed in [25–29].

3.2 Continuous-time dynamics

Over the interval $t \in [t_k^+, t_{k+1}^-]$, the devil-stick will be in flight; its center-of-mass G will undergo projectile motion and its angular momentum will remain conserved. This dynamics is described by the differential equation:

$$\dot{X} = \begin{bmatrix} \omega & 0 & v_x & 0 & v_y & -g \end{bmatrix}^T \tag{3}$$

where the initial condition $X(t_k^+)$ can be obtained from (1) or (2), depending on whether k is odd or even.

3.3 Poincaré sections and half-return maps

For the hybrid system, described by impulsive dynamics of Sect. 3.1 and continuous dynamics of Sect. 3.2, we define two Poincaré sections[2,3] [32] S_r and S_l as follows:

$$\begin{aligned} S_r &: \{X \in \mathbb{R}^6 \mid \theta = \theta^*\} \\ S_l &: \{X \in \mathbb{R}^6 \mid \theta = \pi - \theta^*\} \end{aligned} \tag{4}$$

These Poincaré sections are chosen since the impulsive inputs are applied only when θ is equal to θ^* or $(\pi - \theta^*)$. Any point on S_r and S_l can be described by the vector Y, $Y \subset X$, where

$$Y = \begin{bmatrix} \omega & h_x & v_x & h_y & v_y \end{bmatrix}^T \tag{5}$$

The map $\mathbb{P}_r : S_r \to S_l$ can be determined from (1) and (3) as follows:

$$\begin{aligned} Y(t_{k+1}^-) &= A\, Y(t_k^-) + B_r \\ A &\triangleq \begin{bmatrix} 1 & 0 & 0 & 0 & 0 \\ 0 & 1 & \delta_k & 0 & 0 \\ 0 & 0 & 1 & 0 & 0 \\ 0 & 0 & 0 & 1 & \delta_k \\ 0 & 0 & 0 & 0 & 1 \end{bmatrix}, \\ B_r &\triangleq \begin{bmatrix} (I_k\, r_k/J) \\ -(I_k/m)\sin\theta^*\delta_k \\ -(I_k/m)\sin\theta^* \\ (I_k/m)\cos\theta^*\delta_k - (1/2)g\,\delta_k^2 \\ (I_k/m)\cos\theta^* - g\delta_k \end{bmatrix} \end{aligned} \tag{6}$$

[2] Poincaré sections have been previously used for design of gaits for bipedal robots [30,31]. and orbital stabilization of underactuated systems [27].

[3] It is assumed that the initial conditions of the devil-stick are such that its trajectory intersects one of the two Poincaré sections before the first impulsive control input is applied.

where $\delta_k \triangleq (t_{k+1}^- - t_k^-)$ and $k = (2n-1), n = 1, 2, \cdots$. Similarly, the map $\mathbb{P}_l : S_l \to S_r$ can be determined from (2) and (3) as follows

$$Y(t_{k+1}^-) = A\,Y(t_k^-) + B_l$$
$$B_l \triangleq \begin{bmatrix} -(I_k\, r_k/J) \\ (I_k/m)\sin\theta^*\delta_k \\ (I_k/m)\sin\theta^* \\ (I_k/m)\cos\theta^*\delta_k - (1/2)g\,\delta_k^2 \\ (I_k/m)\cos\theta^* - g\delta_k \end{bmatrix} \tag{7}$$

where $k = 2n, n = 1, 2, \cdots$. Both $\mathbb{P}_r$ and $\mathbb{P}_l$ in (6) and (7), respectively, can be viewed as half-return maps[4] since the composition of these maps are the return maps $\mathbb{P}_r \circ \mathbb{P}_l : S_l \to S_l$ and $\mathbb{P}_l \circ \mathbb{P}_r : S_r \to S_r$. In the next section we introduce a coordinate transformation to show that the map $\mathbb{P}_l$, in the transformed coordinates, is identical to $\mathbb{P}_r$. This simplifies the analysis of the problem.

3.4 Coordinate transformation

Consider Fig. 3, where $z = 0$ denotes the xy plane in which the devil-stick is juggled. Typically, the juggler will stand at a point on the positive z-axis, denoted by P in Fig. 3a, and face the $z = 0$ plane. The juggler will apply a control action with the right hand when $\theta = \theta^*$, and with the left hand when $\theta = \pi - \theta^*$, *i.e.*, the juggler is ambidextrous. Instead of alternating between the right and left hands, the juggler can choose to apply all control actions using the right hand only. This juggler, whom we will now refer to as the handed juggler, will apply the control action standing at P when $\theta = \theta^*$—see– Fig. 3b, and apply the next control action after changing location to Q (mirror image of P) and facing the $z = 0$ plane when $\theta = \pi - \theta^*$—see Fig. 3c. When the devil stick has the orientation $\theta = \pi - \theta^*$, as seen by an observer at P, it will have the orientation $\theta = \theta^*$ for the right-handed juggler. After applying control action at Q, the right-handed juggler will return back to P. If xyz denotes the rotating coordinate frame of the right-handed juggler, the change in position of this juggler can be described by the coordinate transformation:

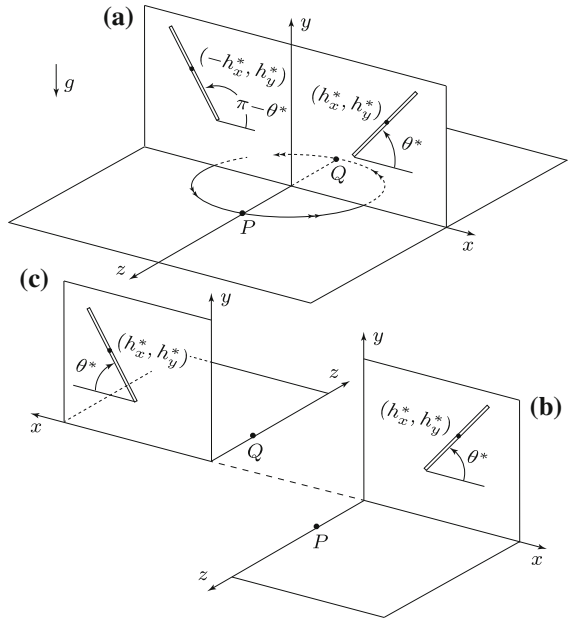

Fig. 3 **a** Ambidexterous juggler standing at P and applying control actions with both hands, **b** right-handed juggler standing at P and applying control action with right hand, **c** right-handed juggler standing at Q and applying control action with right hand

$$\begin{bmatrix} x \\ y \\ z \end{bmatrix}_Q = R_{y,\pi} \begin{bmatrix} x \\ y \\ z \end{bmatrix}_P, \quad \begin{bmatrix} x \\ y \\ z \end{bmatrix}_P = R_{y,\pi} \begin{bmatrix} x \\ y \\ z \end{bmatrix}_Q$$

where

$$R_{y,\pi} \triangleq \text{diag}[-1,\ 1,\ -1]$$

Since $R_{y,\pi}$ changes the sign of the x and z coordinates and leaves the y coordinate unchanged, we can show

$$Y_Q = R\,Y_P, \quad Y_P = R\,Y_Q$$

where

$$R = R^{-1} \triangleq \text{diag}[-1,\ -1,\ -1,\ 1,\ 1]$$

and Y_P and Y_Q denote the vector Y as seen by the right-handed juggler standing at points P and Q, respectively.

[4] Half-return maps have been used to analyze the behavior of dynamical systems such as the van der Pol oscillator [33,34].

3.5 Single return map and discrete-time model

In the reference frame of the right-handed juggler, who alternates between positions P and Q, the two Poincaré sections S_l and S_r are identical, and equal to

$$S : \{X \in \mathbb{R}^6 \ \mid \ \theta = \theta^*\} \tag{8}$$

This follows from our discussion in Sect. 3.4 as well as Fig. 3b, c. The half-return maps $\mathbb{P}_r$ and $\mathbb{P}_l$ in (6) and (7) can be rewritten as follows:

$$Y_P(t_{k+1}^-) = A\, Y_P(t_k^-) + B_r, \quad k = 1, 3, 5, \cdots \tag{9a}$$

$$Y_P(t_{k+1}^-) = A\, Y_P(t_k^-) + B_l, \quad k = 2, 4, 6, \cdots \tag{9b}$$

to explicitly indicate the reference frame of Y. Since the right-handed juggler alternates between positions P and Q, the half-return map $\mathbb{P}_l$ in (9b) can be transformed as follows:

$$\begin{aligned} & RY_P(t_{k+1}^-) = RA\, Y_P(t_k^-) + RB_l \\ \Rightarrow \quad & Y_Q(t_{k+1}^-) = AR\, Y_P(t_k^-) + RB_l \\ \Rightarrow \quad & Y_Q(t_{k+1}^-) = A\, Y_Q(t_k^-) + B_r, \quad k = 2, 4, 6, \cdots \end{aligned} \tag{10}$$

where we used the relations $RA = AR$ and $RB_l = B_r$. It is clear from (9a) and (10) that the half-return maps $\mathbb{P}_r$ and $\mathbb{P}_l$ in (6) and (7) are identical in the reference frame of the right-handed juggler. This implies that the hybrid dynamics of the devil-stick between any two control actions can be described by a single return map if the change in reference frame of the right-handed juggler is incorporated in the dynamic model. This map, $\mathbb{P} : S \to S$, can be obtained by first rewriting (9a) and (10) as follows:

$$\begin{aligned} & RY_Q(t_{k+1}^-) = A\, Y_P(t_k^-) + B_r, && k = 1, 3, 5, \cdots \\ \Rightarrow \quad & Y_Q(t_{k+1}^-) = R\left[A\, Y_P(t_k^-) + B_r\right], && k = 1, 3, 5, \cdots \end{aligned} \tag{11a}$$

$$\begin{aligned} & RY_P(t_{k+1}^-) = A\, Y_Q(t_k^-) + B_r, && k = 2, 4, 6, \cdots \\ \Rightarrow \quad & Y_P(t_{k+1}^-) = R\left[A\, Y_Q(t_k^-) + B_r\right], && k = 2, 4, 6, \cdots \end{aligned} \tag{11b}$$

Then, by accounting for the change in reference frame of the right-handed juggler after each control action, (11a) and (11b) can be combined into the following single equation which represents the return map $\mathbb{P}$:

$$\bar{Y}(t_{k+1}^-) = R\left[A\bar{Y}(t_k^-) + B_r\right], \qquad k = 1, 2, 3, \cdots$$

where $\bar{Y}$ denotes the state vector Y in the reference frame of the right-handed juggler. The above equation results in the following discrete-time equations:

$$\omega(t_{k+1}^-) = -\omega(t_k^-) - (I_k\, r_k/J) \tag{12a}$$

$$h_x(t_{k+1}^-) = -h_x(t_k^-) - \left[v_x(t_k^-) - (I_k/m)\sin\theta^*\right]\delta_k \tag{12b}$$

$$v_x(t_{k+1}^-) = -v_x(t_k^-) + (I_k/m)\sin\theta^* \tag{12c}$$

$$\begin{aligned} h_y(t_{k+1}^-) = {} & h_y(t_k^-) - (1/2)g\,\delta_k^2 \\ & + \left[v_y(t_k^-) + (I_k/m)\cos\theta^*\right]\delta_k \end{aligned} \tag{12d}$$

$$v_y(t_{k+1}^-) = v_y(t_k^-) + (I_k/m)\cos\theta^* - g\,\delta_k \tag{12e}$$

where $\delta_k \triangleq (t_{k+1}^- - t_k^-)$, $k = 1, 2, \cdots$, is the time of flight between two consecutive control actions. During this time duration, the devil-stick rotates by a net angle $\pi - 2\theta^*$. Since the angular velocity of the stick remains constant in the interval $[t_k^+, t_{k+1}^-]$, δ_k is given as follows

$$\delta_k = \frac{\Delta\theta}{\omega(t_k^-) + (I_k\, r_k/J)}, \quad \Delta\theta \triangleq (\pi - 2\theta^*) \tag{13}$$

The control design for juggling is presented next.

4 State feedback control design

4.1 Steady-state dynamics

From the discussion in Sect. 3.5 it becomes clear that when the change of reference frame of the juggler is taken into account, the problem of juggling between the two distinct configurations (θ^*, h_x^*, h_y^*) and $(\pi - \theta^*, -h_x^*, h_y^*)$ is converted to the problem of juggling between identical configurations (θ^*, h_x^*, h_y^*) and (θ^*, h_x^*, h_y^*). If the state variables at this configuration are denoted by

$$\bar{Y}^* \triangleq \left[\omega^*\ h_x^*\ v_x^*\ h_y^*\ v_y^*\right]^T \tag{14}$$

then $\bar{Y}^* = \mathbb{P}(\bar{Y}^*)$ is a fixed point and (12) and (13) give

$$\omega^* = -\omega^* - (I_k^*\, r_k^*/J) \tag{15a}$$

$$h_x^* = -h_x^* - \left[v_x^* - (I_k^*/m)\sin\theta^*\right]\delta^* \tag{15b}$$

$$v_x^* = -v_x^* + (I_k^*/m)\sin\theta^* \tag{15c}$$

$$h_y^* = h_y^* - (1/2)g\,\delta^{*2} + \left[v_y^* + (I_k^*/m)\cos\theta^*\right]\delta^* \tag{15d}$$

$$v_y^* = v_y^* + (I_k^*/m)\cos\theta^* - g\,\delta^* \tag{15e}$$

$$\delta^* = \frac{\Delta\theta}{\omega^* + (I_k^*\, r_k^*/J)} \tag{15f}$$

where I_k^*, r_k^* denote the steady-state values of the control inputs and δ^* denote the steady-state value of the time of flight. Since h_y^* is eliminated from (15d), (15) represents six equations in seven unknowns, namely, ω^*, h_x^*, v_x^*, v_y^*, I^*, r^*, and δ^*. By choosing δ^*, the remaining six unknowns are obtained as follows:

$$\begin{aligned} \omega^* &= -\Delta\theta/\delta^*, & h_x^* &= g\,\delta^{*2}\tan\theta^*/4 \\ v_x^* &= g\,\tan\theta^*\delta^*/2, & v_y^* &= -g\,\delta^*/2 \\ I^* &= mg\delta^*/\cos\theta^*, & r^* &= 2J\cos\theta^*\Delta\theta/(mg\delta^{*2}) \end{aligned} \tag{16}$$

Since the point of application of the impulsive force must lie on the stick, r^* in (16) must satisfy $0 < r^* < \ell/2$. This imposes the following constraint of the value of δ^*:

$$\delta^* > \bar{\delta}, \quad \bar{\delta} \triangleq 2\sqrt{\frac{J\cos\theta^*\Delta\theta}{mg\ell}} \tag{17}$$

It should be noted that for a given value of δ^*, the value of h_y^* is not unique.

4.2 Error dynamics

To converge the states to their desired values, we first define the discrete error variables:

$$\begin{aligned} \widetilde{\omega}(k) &\triangleq \omega(t_k^-) - \omega^* \\ \widetilde{h}_x(k) &\triangleq h_x(t_k^-) - h_x^*, & \widetilde{v}_x(k) &\triangleq v_x(t_k^-) - v_x^* \\ \widetilde{h}_y(k) &\triangleq h_y(t_k^-) - h_y^*, & \widetilde{v}_y(k) &\triangleq v_y(t_k^-) - v_y^* \\ \widetilde{u}_1(k) &\triangleq (I_k r_k - I^* r^*)/J, & \widetilde{u}_2(k) &\triangleq (I_k - I^*)/m \end{aligned} \tag{18}$$

Using (12) and (15a)–(15e), the error dynamics can now be written as

$$\widetilde{\omega}(k+1) = -\widetilde{\omega}(k) - \widetilde{u}_1(k) \tag{19a}$$

$$\widetilde{h}_x(k+1) = -\widetilde{h}_x(k) - \delta_k\widetilde{v}_x(k) + \delta_k\sin\theta^*\,\widetilde{u}_2(k) \tag{19b}$$

$$\widetilde{v}_x(k+1) = -\widetilde{v}_x(k) + \sin\theta^*\,\widetilde{u}_2(k) \tag{19c}$$

$$\widetilde{h}_y(k+1) = \widetilde{h}_y(k) + \delta_k\widetilde{v}_y(k) + \delta_k\cos\theta^*\,\widetilde{u}_2(k) + (g/2)\left[\delta_k\delta_k^* - \delta_k^2\right] \tag{19d}$$

$$\widetilde{v}_y(k+1) = \widetilde{v}_y(k) + \cos\theta^*\widetilde{u}_2(k) - g\,[\delta_k - \delta_k^*] \tag{19e}$$

where δ_k, defined in (13), can be written in terms of the error variables as follows:

$$\delta_k = \frac{\Delta\theta\,\delta^*}{[\widetilde{\omega}(k) + \widetilde{u}_1(k)]\,\delta^* + \Delta\theta} \tag{20}$$

It is clear from (19) and (20) that the error dynamics is nonlinear. In the next section we present a partial control design that converts the nonlinear system into a linear system and simplifies the remaining control design.

4.3 Partial control design: dead-beat control

The error dynamics in (19) involves two control inputs, namely, $\widetilde{u}_1(k)$ and $\widetilde{u}_2(k)$. The input $\widetilde{u}_1(k)$ appears only in (19a). To this end, we first design $\widetilde{u}_1(k)$ as follows:

$$\widetilde{u}_1(k) = -\widetilde{\omega}(k) \tag{21}$$

to guarantee dead-beat convergence[5] of the error state $\widetilde{\omega}(k)$. Substitution of (21) in (20) yields $\delta_k = \delta^*$. Since δ^* is user-defined and is a constant, the choice of control in (21) is special as it transforms the remaining dynamics in (19b)–(19e) into the linear system:

$$\begin{aligned} z(k+1) &= \mathcal{A}\,z(k) + \mathcal{B}\,\widetilde{u}_2(k) \\ z(k) &\triangleq \left[\widetilde{h}_x(k)\ \widetilde{v}_x(k)\ \widetilde{h}_y(k)\ \widetilde{v}_y(k)\right]^T \\ \mathcal{A} &\triangleq \begin{bmatrix} -1 & -\delta^* & 0 & 0 \\ 0 & -1 & 0 & 0 \\ 0 & 0 & 1 & \delta^* \\ 0 & 0 & 0 & 1 \end{bmatrix}, \quad \mathcal{B} \triangleq \begin{bmatrix} \delta^*\sin\theta^* \\ \sin\theta^* \\ \delta^*\cos\theta^* \\ \cos\theta^* \end{bmatrix} \end{aligned} \tag{22}$$

It can be verified that the pair $(\mathcal{A}, \mathcal{B})$ is controllable since $\theta^* \in (0, \pi/2)$ and $\delta^* > 0$.

4.4 Residual control design

The error dynamics in (22) is linear and therefore a linear controller can be designed to converge the states

[5] It should be noted that dead-beat inputs have been used in earlier works on juggling [8,11,17].

to the origin. However, it should be noted that the control input $\widetilde{u}_2(k)$ determines the value of I_k which also appears in the dead-beat control design $\widetilde{u}_1(k)$—see (18). By using the values of $\widetilde{u}_2(k)$ from (18) in (21), we get:

$$r_k = \left[I^* r^* - J\widetilde{\omega}(k)\right]/I_k \tag{23}$$

Since the point of application of impulsive force must lie of the stick, r_k must satisfy $-\ell/2 < r_k < \ell/2$. By imposing this condition on the value of r_k in (23), we get the following constraints on the input $\widetilde{u}_2(k)$:

$$\begin{aligned} \widetilde{u}_2(k) &> \left[2I^* r^* - 2J\widetilde{\omega}(k) - I^*\ell\right]/(m\ell) \\ \widetilde{u}_2(k) &> \left[-2I^* r^* + 2J\widetilde{\omega}(k) - I^*\ell\right]/(m\ell) \end{aligned} \tag{24}$$

Since I^* and r^* are both positive, as it can be seen from (16), the inequalities in (24) can be combined into the single inequality:

$$\begin{aligned} &\widetilde{u}_2(k) > \bar{a} + \bar{b}\,|\widetilde{\omega}(k)\,| \\ &\bar{a} \triangleq (2r^* - \ell)I^*/(m\ell), \quad \bar{b} \triangleq 2J/(m\ell) \end{aligned} \tag{25}$$

Since $\widetilde{u}_1(k)$ is dead-beat, $\widetilde{\omega}(k) = 0, k = 2, 3\cdots$. Thus, (25) can also be written as

$$\begin{aligned} &\widetilde{u}_2(k) > \bar{a} + \bar{b}\,|\widetilde{\omega}(k)\,|, && k = 1 \\ &\widetilde{u}_2(k) > \bar{a}, && k = 2, 3, \cdots \end{aligned} \tag{26}$$

The input $\widetilde{u}_2(k)$ is designed using Linear Quadratic Regulator (LQR) and Model Predictive Control (MPC) methods. For an LQR design, the control minimizes the cost function

$$J = \sum_{k=1}^{\infty} \left[z(k)^T Q\, z(k) + R\,\widetilde{u}_2^2(k)\right] \tag{27}$$

where, Q and R are constant weighting matrices that can be chosen by trial and error to satisfy the constraints in (26). The closed-form solution of the control input $\widetilde{u}_2(k)$ can be obtained by solving the Ricatti equation [35].

For a receding horizon MPC design, the constraint in (26) can be explicitly included in the optimization problem. In the MPC design[6], it is necessary to calculate the predicted output with future control input as the adjusted variable. Since the current control input cannot affect the output at the same time for receding horizon control, the system dynamics must be represented in terms of the difference between the current and the predicted control input. To this end, we define the following variables based on the augmented state-space model[7] in [36]:

$$\begin{aligned} &\Delta u(k_i) \triangleq \widetilde{u}_2(k_i) - \widetilde{u}_2(k_i - 1) \\ &\Delta U_i \triangleq \begin{bmatrix} \Delta u(k_i) \\ \Delta u(k_i + 1) \\ \vdots \\ \Delta u(k_i + N_c - 1) \end{bmatrix}, \\ &Z_i \triangleq \begin{bmatrix} z(k_i + 1 \mid k_i) \\ z(k_i + 2 \mid k_i) \\ \vdots \\ z(k_i + N_p \mid k_i) \end{bmatrix} \end{aligned} \tag{28}$$

where k_i is the current sampling instant, $z(k_i)$ is the state vector in (22) measured at k_i, N_c is the control horizon, N_p is the prediction horizon, and $z(k_i + m \mid k_i)$ is the predicted state variable at $k_i + m$ with state measurements $z(k_i)$.

We now construct the following N-step receding horizon optimal control problem:

$$\text{minimize } J = \sum_{i=1}^{N} \left[Z_i^T Z_i + \Delta U_i^T \Delta U_i\right] \tag{29}$$

subject to

$$\begin{aligned} &z(k_i + 1) = \mathcal{A}\, z(k_i) + \mathcal{B}\,\widetilde{u}_2(k_i) \\ &\widetilde{u}_2(k_i) > \bar{a} + \bar{b}\,|\widetilde{\omega}(1)\,|, && i = 1 \\ &\widetilde{u}_2(k_i) > \bar{a}, && i = 2, 3\cdots, N \end{aligned} \tag{30}$$

In every sampling period, the optimization problem determines the best control parameter ΔU_i that attempts to converge the sequence of states in Z_i to zero. Although ΔU_i contains N_c number of future control inputs, only the first entry is implemented as the actual control input. This optimization process is repeated using a more recent measurement of the states. It should be emphasized that the input constraint in (30), namely, $\widetilde{u}_2(k_i) > \bar{a} + \bar{b} \mid \widetilde{\omega}(1) \mid$ is imposed only in the first optimization window. In subsequent optimization windows, the constraint is relaxed to $\widetilde{u}_2(k_i) > \bar{a}$.

[6] A detailed discussion of MPC design for discrete-time systems can be found in Chapters 1-3 in [36].

[7] The augmented state-space model is controllable; this was verified using Theorem 1.2 in [36].

This is necessary for $\widetilde{u}_2$ to converge to zero since $\bar{a}$ is negative—see (25), whereas $\bar{a} + \bar{b}\,|\,\widetilde{\omega}(1)\,|$ can assume positive values based on the initial value of $\widetilde{\omega}$.

Remark 1 The control input $\widetilde{u}_2(k)$ is obtained as the numerical solution of the optimal control problem in (29) and (30). These inputs are applied at discrete time instants and the optimization solver is required to compute these inputs within the sampling time interval, which is equal to the time of flight δ^*. Since δ^* is relatively large, there is sufficient time for the optimization solver to generate the solution. This, along with the fact that the input constraint can be explicitly considered in the problem formulation, makes MPC well-suited for this problem.

5 Simulation results

5.1 System parameters and initial conditions

We present simulation results of both LQR- and MPC-based control designs. The physical parameters of the devil-stick are provided below in SI units:

$$m = 0.1, \quad \ell = 0.5, \quad J = 0.0021 \tag{31}$$

Using these physical parameters and by choosing the values of $\theta^* = \pi/6$ rad and $\delta^* = 0.5$ sec, the steady-state values of state variables and control inputs are obtained from (16) as

$$\begin{aligned} &\omega^* = -4.18\,\text{rad/s} \quad && h_x^* = 0.353\,\text{m} \quad && v_x^* = 1.414\,\text{m/s} \\ &v_y^* = -2.45\,\text{m/s} && I^* = 0.565\,\text{Ns} && r^* = 0.030\,\text{m} \end{aligned} \tag{32}$$

Since h_y^* can be chosen arbitrarily, we chose

$$h_y^* = 3.0\,\text{m} \tag{33}$$

At the initial time, we assume $\theta = \theta^* = \pi/6$ rad and the states variables (in SI units) are

$$\begin{aligned} &\omega(0) = 0, \quad h_x(0) = 0.53, \quad v_x(0) = 2.0 \\ &h_y(0) = 1.0, \quad v_y(0) = -2.0 \end{aligned} \tag{34}$$

For the physical parameters in (31), steady-state values of the states in (32) and (33), and initial conditions in (34), the control $\widetilde{u}_1(k)$ was chosen according to (21). The control input $\widetilde{u}_2(k)$ was designed using LQR and MPC methods and simulation results are presented next.

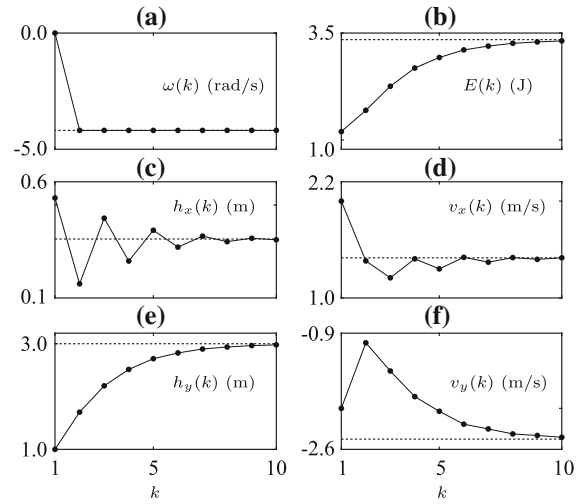

Fig. 4 State variables and total energy E of the devil-stick at sampling instants k, $k = 1, 2, \cdots, 10$, for the LQR design

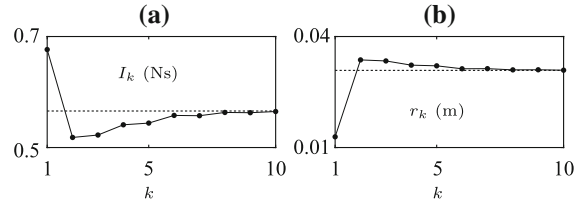

Fig. 5 Control inputs for the devil-stick at sampling instants k, $k = 1, 2, \cdots, 10$, for the LQR design

5.2 Results for the LQR-based design

For the LQR design, the weight matrix Q for the states was chosen to be the identity matrix and the control weight R was chosen as 0.2. The control was obtained as

$$\widetilde{u}_2(k) = Fz(k), \quad F = \begin{bmatrix} -0.43 & -0.77 & 0.43 & 0.66 \end{bmatrix} \tag{35}$$

The simulation results are shown in Figs. 4[8] and 5 . It can be seen from Fig. 4a that the dead-beat control $\widetilde{u}_1(k)$ converges $\omega(k)$ to ω^* in one sampling interval. The control $\widetilde{u}_2(k)$ converges the remaining states to their steady-state values given in (32) in approximately $k = 10$ steps—see Fig. 4c–f. The control inputs I_k and r_k are shown in Fig. 5a, b. It can be seen that both control inputs converge to their steady-state values defined

[8] It should be noted that the state variables are shown in the reference frame of the right-handed juggler.

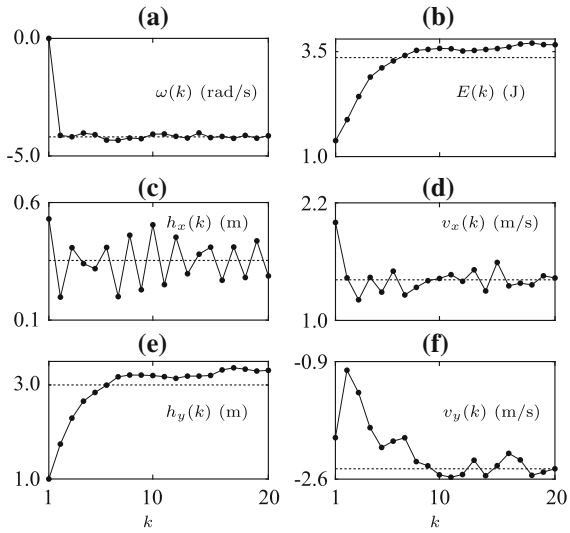

Fig. 6 State variables and total energy E of the devil-stick at sampling instants k, $k = 1, 2, \cdots, 20$, for the LQR design in the presence of parameter uncertainty, sensor noise and input disturbance

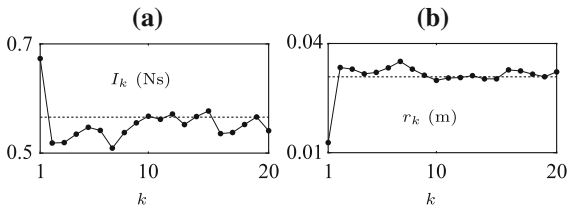

Fig. 7 Control inputs for the devil-stick at sampling instants k, $k = 1, 2, \cdots, 20$, for the LQR design in the presence of parameter uncertainty, sensor noise and input disturbance

in (32); also the control input r_k remains well inside the constraint boundary $|\, r_k \,| < \ell/2$. The convergence of both the states and control inputs to their desired values imply that the devil-stick is juggled between two symmetric configurations. Since the magnitudes of v_x, v_y, ω_x, and h_y are the same in the two symmetric configurations, the total energy E (kinetic plus potential) reaches a constant value at steady state—see Fig. 4b.

Remark 2 The total energy of the devil-stick is the same at the symmetric configurations. Also, it is conserved during the flight phase. Therefore, in steady-state, the control inputs I^* and r^* do zero work on the system.

The behavior of the devil-stick was also simulated in the presence of parameter uncertainty, sensor noise, and input disturbance. For the same initial conditions in (34) and controller gains in (35), the results are shown in Figs. 6 and 7. In the dynamic model, the values of the mass m and length ℓ were purposely chosen to be 2% less and 2% more, respectively, than the values provided in (31). The velocity measurements, which are used to compute the control inputs $\widetilde{u}_1(k)$ and $\widetilde{u}_2(k)$ in (21) and (35), were corrupted by random noise in the range of $\pm 2\%$ of the actual values. Random noise in the range of $\pm 2\%$ was also added to the computed values of the physical inputs I_k and r_k to simulate input disturbance. It is clear from Figs. 5 and 7 that the inputs I_k and r_k are significantly perturbed from their nominal values; this is because of the combined effect of measurement noise and input disturbance. Despite the large perturbations in the physical inputs from their nominal values, it can be seen from Fig. 6 that the states of the system become ultimately bounded in a neighborhood of their desired values. The state ω is bounded in a small neighborhood of its desired value as $\tilde{u}_1(k)$ is not exactly dead-beat. Among the other states, h_x, v_x and v_y oscillate around their respective desired values but h_y oscillates around a higher value, mainly because of the higher value of the mass parameter used in the control law. Since the potential energy of the devil-stick is proportional the state h_y, the energy E also oscillates around a value that is higher than its desired value. The simulation was carried out for a longer period of time than shown; the results indicate stable behavior with ultimate boundedness of the state trajectories.

5.3 Results for the MPC-based design

The control horizon, prediction horizon, and the number of steps were taken as

$$N_c = 5, \quad N_p = 10, \quad N = 15$$

The MPC problem, defined by (29) and (30) were solved using quadratic programming in MATLAB[9]. The state variables $h_x(k)$, $h_y(k)$, $v_x(k)$ and $v_y(k)$ and the control inputs I_k and r_k are shown in Fig. 8. The state variable $\omega(k)$ is not shown as it converged to its desired value in one sampling interval by the dead-beat controller. Similar to the LQR design, the control input r_k remains well inside the constraint boundary. The trajectory of the center-of-mass of the devil stick is shown in Fig. 9a; it starts from the initial configuration $(h_x, h_y) = (0.53, 1.00)$ and is eventually juggled between the symmetric coordinates $(h_x^*, h_y^*) =$

[9] The quadprog MATLAB function was used.

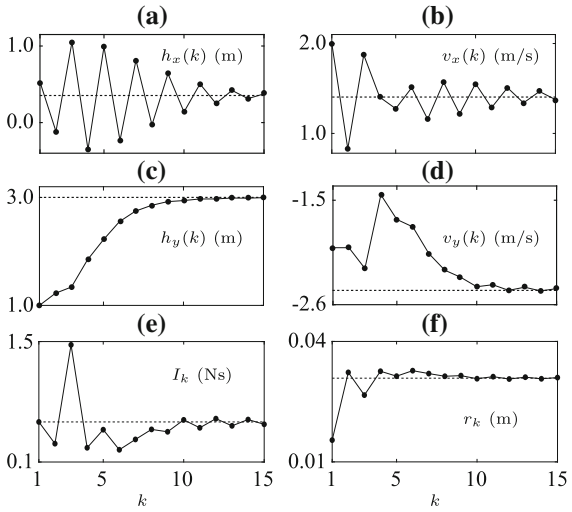

Fig. 8 State variables and control inputs of the devil-stick at sampling instants k, $k = 1, 2, \cdots, 15$, for the MPC design

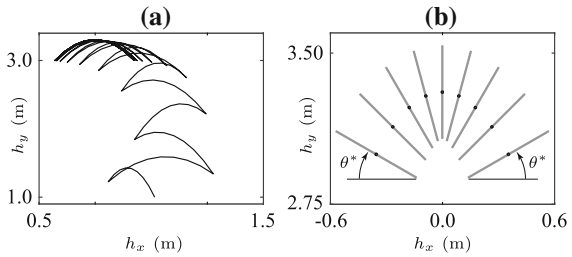

Fig. 9 **a** Trajectory of the center-of-mass from the initial configuration to steady-state and **b** symmetric configurations and seven intermediate configurations of the devil-stick in steady state for the MPC design

$(0.353, 3.00)$, $(-h_x^*, h_y^*) = (-0.353, 3.00)$ in steady state. Typically, N is chosen to be large to guarantee convergence. For our system, the states rapidly converged to zero with $N = 15$. In Fig. 9b, the devil-stick is shown at the two symmetric configurations where $\theta^* = \pi/6$ and several intermediate configurations that are equal time intervals apart.

Remark 3 In all the simulations, the stick rotates by an angle $(\pi - 2\theta^*)$ between two consecutive control inputs. This corresponds to "top-only idle" juggling [1]. The dynamic model and control design are quite general and the stick can be controlled to rotate by $(q\pi - 2\theta^*)$, $q = 2, 3, \cdots$, by simply changing the definition of $\Delta\theta$ in (13) from $\Delta\theta = (\pi - 2\theta^*)$ to $\Delta\theta = (q\pi - 2\theta^*)$. In other words, the stick can be made to flip multiple times in the flight phase, if desired. The "flip-idle" in [1] corresponds to the case where $q = 2$.

6 Conclusion

Impulsive forces are applied intermittently for juggling a devil-stick between two symmetric configurations. A dynamic model of the devil-stick and a control design for the juggling task is presented here for the first time. The control inputs are the impulse of the impulsive force and its point of application on the stick. The control action is event-based and the inputs are applied only when the stick has the orientation of one of the two symmetric configurations. The dynamics of the devil-stick due to the control action and torque-free motion under gravity is described by two Poincaré maps; the symmetric configurations are fixed points of the corresponding Poincaré sections. A coordinate transformation is used to exploit the symmetry and convert the problem into that of stabilization of a single fixed point. A dead-beat controller is designed to convert the nonlinear system into a controllable linear discrete-time system with input constraints. LQR and MPC methods are used to design the control inputs and achieve symmetric juggling. The LQR method has a closed-form solution and is easier to implement but requires trial and error to satisfy the input constraints. The MPC method has no closed-form solution as it is obtained by solving an optimization problem online. However, the optimization problem directly takes into account the input constraint. The computational cost of the MPC method, which can be a concern for many problems, is not a concern for the juggling problem since the time between consecutive control actions is relatively large. Simulation results validate both control designs and demonstrate non-prehensile manipulation solely using impulsive forces. For the LQR controller, the closed-loop system is shown to have some degree of robustness to parameter uncertainty, measurement noise, and input disturbance. Our future work will focus on robotic juggling; this includes design of experimental hardware, adaptive compensation of energy losses due to inelastic collisions between the devil-stick and hand sticks, and motion planning and control of the robot end-effector for generating the impulsive forces designed by the control algorithms. In this regard, the works by Brogliato and co-authors on complete control design of both the manipulator and the juggled object [8,11] and adaptive control [17] will provide useful clues.

Acknowledgements The authors acknowledge the support provided by the National Science Foundation, Grant CMMI-1462118.

Compliance with ethical standards

Conflict of interest The authors declare that they do not have any conflict of interest.

References

1. HNWpodcasts. Five easy devil stick tricks with instructions. https://www.youtube.com/watch?v=Z7Pv-p-nEYo, (2013). [Online Accessed 01 May 2020]
2. Duinker, N.: Devilstick tutorial—basic tricks to get you started. https://www.youtube.com/watch?v=MAuAtwZ7BF4, (2015). [Online Accessed 01 May 2020]
3. Lynch, K.M., Mason, M.T.: Dynamic underactuated nonprehensile manipulation. In Proceedings of IEEE/RSJ international conference on intelligent robots and systems. IROS'96. IEEE, vol 2, pp 889–896 (1996)
4. Lynch, K.M., Mason, M.T.: Dynamic nonprehensile manipulation: controllability, planning, and experiments. Int. J. Robot. Res. **18**(1), 64–92 (1999)
5. Lynch, K.M., Murphey, T.D.: Control of nonprehensile manipulation. In: Control problems in robotics. Springer, pp 39–57(2003)
6. Mason, M.T.: Progress in nonprehensile manipulation. Int. J. Robot. Res. **18**(11), 1129–1141 (1999)
7. Woodruff, J.Z., Lynch, K.M.: Planning and control for dynamic, nonprehensile, and hybrid manipulation tasks. In: 2017 IEEE international conference on robotics and automation (ICRA). IEEE, pp 4066–4073 (2017)
8. Brogliato, B., Rio, A.Z.: On the control of complementary-slackness juggling mechanical systems. IEEE Trans. Autom. Control **45**(2), 235–246 (2000)
9. Hirai, H., Fumio, M.: Dynamic coordination between robots: self-organized timing selection in a juggling-like ball-passing task. IEEE Trans. Syst. Man Cybern. Part B (Cybernetics) **36**(4), 738–754 (2006)
10. Kober, J., Glisson, M., Mistry, M.: Playing catch and juggling with a humanoid robot. In: 12th IEEE-RAS international conference on humanoid robots (Humanoids 2012). IEEE, pp 875–881 (2012)
11. Zavala-Rio, A.: Brogliato, Bernard: on the control of a one degree-of-freedom juggling robot. Dyn. Control **9**(1), 67–90 (1999)
12. Brogliato, B.: Feedback control of multibody systems with joint clearance and dynamic backlash: a tutorial. Multibody Syst. Dyn. **42**(3), 283–315 (2018)
13. Brogliato, B., Mabrouk, M., Rio, A.Z.: On the controllability of linear juggling mechanical systems. Syst. Control Lett. **55**(4), 350–367 (2006)
14. Goebel, R., Sanfelice, Ricardo, G., Teel, Andrew R.: Hybrid dynamical systems: modeling stability, and robustness, (2012)
15. Lynch, K.M., Black, C.K.: Recurrence, controllability, and stabilization of juggling. IEEE Trans. Robot. Autom. **17**(2), 113–124 (2001)
16. Tornambe, Antonio: Modeling and control of impact in mechanical systems: theory and experimental results. IEEE Trans. Autom. Control **44**(2), 294–309 (1999)
17. Zavala-Rio, A., Brogliato, B.: Direct adaptive control design for one-degree-of-freedom complementary-slackness jugglers. Automatica **37**(7), 1117–1123 (2001)
18. Ronsse, R., Lefevre, P., Sepulchre, R.: Rhythmic feedback control of a blind planar juggler. IEEE Trans. Robot. **23**(4), 790–802 (2007)
19. Sanfelice, R.G., Teel, A.R., Sepulchre, R.: A hybrid systems approach to trajectory tracking control for juggling systems. In: 46th IEEE conference on decision and control. IEEE, pp 5282–5287 (2007)
20. Schaal, S., Atkeson, C.G.: Open loop stable control strategies for robot juggling. In: Proceedings IEEE international conference on robotics and automation. IEEE, pp 913–918 (1993)
21. Spong, M.W.: Impact controllability of an air hockey puck. Syst. Control Lett. **42**(5), 333–345 (2001)
22. Nakaura, S., Yasuyuki, K., Tadasuke, M., Mitsuji, S.: Enduring rotary motion control of devil stick. IFAC Proc. Vol. **37**(13), 805–810 (2004)
23. Shiriaev, A., Robertsson, A., Freidovich, L., Johansson, R.: Generating stable propeller motions for devil stick. In: 3rd IFAC workshop on Lagrangian and Hamiltonian methods for nonlinear control, 2006, (2006)
24. Brogliato, B.: Nonsmooth Mechanics. Models Dynamics and Control. Springer Nature, Switzerland AG (2016)
25. Kant, N., Mukherjee, R., Khalil, H. K.: Stabilization of homoclinic orbits of two degree-of-freedom underactuated systems. In: 2019 American Control Conference (ACC), (2019)
26. Kant, N., Ranjan, M.: Impulsive dynamics and control of the inertia-wheel pendulum. IEEE Robot. Autom. Lett. **3**(4), 3208–3215 (2018)
27. Kant, N., Mukherjee, R.: Orbital stabilization of underactuated systems using virtual holonomic constraints and impulse controlled Poincaré maps. Syst. Control Lett. **146**, 104813 (2020)
28. Kant, N., Mukherjee, R., Chowdhury, D., Khalil, H.K.: Estimation of the region of attraction of underactuated systems and its enlargement using impulsive inputs. In: IEEE transactions on robotics, pp 1–15, (2019)
29. Mathis, F.B., Rouhollah, J., Mukherjee, R.: Impulsive actuation in robot manipulators: experimental verification of pendubot swing-up. IEEE/ASME Trans. Mechatron. **19**(4), 1469–1474 (2014)
30. Grizzle, J.W., Abba, G., Plestan, F.: Asymptotically stable walking for biped robots: analysis via systems with impulse effects. IEEE Trans. Autom. Control **46**(1), 51–64 (2001)
31. Westervelt, E.R., Grizzle, J.W., Koditschek, D.E.: Hybrid zero dynamics of planar biped walkers. IEEE Trans. Autom. Control **48**(1), 42–56 (2003)
32. Wiggins, S.: Introduction to Applied Nonlinear Dynamical Systems and Chaos. Springer Science & Business Media, Berlin (2003)

33. Bold, K., Edwards, C., Guckenheimer, J., Guharay, S., Hoffman, K., Hubbard, J., Oliva, R., Weckesser, W.: The forced van der Pol equation II: canards in the reduced system. SIAM J. Appl. Dyn. Syst. **2**(4), 570–608 (2003)
34. Guckenheimer, J., Hoffman, K., Weckesser, W.: The forced van der Pol equation I: the slow flow and its bifurcations. SIAM J. Appl. Dyn. Syst. **2**(1), 1–35 (2003)
35. Antsaklis, P.J., Michel, A.N.: A Linear Systems Primer. Birkhauser, Basel (2007)
36. Wang, L.: Model Predictive Control System Design and Implementation Using MATLAB. Springer Science & Business Media, Berlin (2009)